Journal of Inorganic Biochemistry 257 (2024) 112583

Contents lists available at ScienceDirect

Journal of Inorganic Biochemistry

journal homepage: www.elsevier.com/locate/jinorgbio

Preparation and characterization of $Mn^{II}Mn^{III}$ complexes with relevance to class Ib ribonucleotide reductases

Lorna M. Doyle [a], Roel L.M. Bienenmann [a,1], Robert Gericke [a,2], Shuangning Xu [b], Erik R. Farquhar [c], Lawrence Que Jr [b], Aidan R. McDonald [a,*]

[a] School of Chemistry, Trinity College Dublin, The University of Dublin, College Green, Dublin 2, Ireland
[b] Department of Chemistry and Centre for Metals in Biocatalysis, University of Minnesota, Minneapolis, 55455 MN, United States
[c] Case Western Reserve University Center for Synchrotron Biosciences, National Synchrotron Light Source II, Brookhaven National Laboratory Upton, NY, 11973 New York, United States

ARTICLE INFO

Keywords:
Bioinorganic
Dimanganese cluster
Ribonucleotide reductase
Dioxygen activation
electron paramagnetic resonance

ABSTRACT

The Mn_2 complex $[Mn^{II}_2(TPDP)(O_2CPh)_2](BPh_4)$ (**1**, TPDP = 1,3-bis(bis(pyridin-2-ylmethyl)amino)propan-2-ol, Ph =phenyl) was prepared and subsequently characterized via single-crystal X-ray diffraction, X-ray absorption, electronic absorption, and infrared spectroscopies, and mass spectrometry. **1** was prepared in order to explore its properties as a structural and functional mimic of class Ib ribonucleotide reductases (RNRs). **1** reacted with superoxide anion ($O_2^{\bullet-}$) to generate a peroxido-$Mn^{II}Mn^{III}$ complex, **2**. The electronic absorption and electron paramagnetic resonance (EPR) spectra of **2** were similar to previously published peroxido-$Mn^{II}Mn^{III}$ species. Furthermore, X-ray near edge absorption structure (XANES) studies indicated the conversion of a Mn^{II}_2 core in **1** to a $Mn^{II}Mn^{III}$ state in **2**. Treatment of **2** with *para*-toluenesulfonic acid (*p*-TsOH) resulted in the conversion to a new $Mn^{II}Mn^{III}$ species, **3**, rather than causing O—O bond scission, as previously encountered. **3** was characterized using electronic absorption, EPR, and X-ray absorption spectroscopies. Unlike other reported peroxido-$Mn^{II}Mn^{III}$ species, **3** was capable of oxidative O—H activation, mirroring the generation of tyrosyl radical in class Ib RNRs, however *without* accessing the $Mn^{III}Mn^{IV}$ state.

1. Introduction

Ribonucleotide reductase (RNRs) are metalloenzymes that catalyze the conversion of ribonucleotides to the corresponding deoxyribonucleotides. [1–4] This represents the initial and rate limiting step in deoxyribonucleic acid (DNA) synthesis and repair in all organisms. RNRs are divided into five subclasses depending on the metals in their active site, their activating oxidants, and the radical species generated during the catalytic cycle. [4] The sub-class Ib RNRs contain a dimanganese (Mn_2) cofactor, which is putatively activated using superoxide ($O_2^{\bullet-}$) as an oxidant, and generates a tyrosyl radical species upon oxidation of a nearby tyrosine. The tyrosyl radical triggers a long-distance thiyl radical generation that facilitates ribonucleotide activation. In the proposed catalytic cycle for the Mn_2 core in class Ib RNRs (Scheme 1), O_2 reacts with a nearby flavodoxin protein (a hydroquinone - $NrdI_{hq}$) to form $O_2^{\bullet-}$. [5] $O_2^{\bullet-}$ is postulated to react with the reduced Mn^{II}_2 core yielding a peroxido-$Mn^{II}Mn^{III}$ species that converts to a bis(μ-oxo) $Mn^{III}Mn^{IV}$ entity. The $Mn^{III}Mn^{IV}$ species is postulated to be the oxidant that activates tyrosine to produce a tyrosyl radical which subsequently initiates ribonucleotide reduction.

The role of H^+-donors in this cycle is not clear – it is possible that peroxide and/or oxo-ligands are protonated, or that H^+-donors trigger O—O and/or O—H bond activation. Stubbe and co-workers postulated that $O_2^{\bullet-}$ may react with the Mn^{II}_2 core as $HO_2^{\bullet}$ rather than the free $O_2^{\bullet-}$ anion, which would yield a hydroperoxido-$Mn^{II}Mn^{III}$. [5] It has also been proposed that proton-mediated O—O bond activation occurs at a Mn-bound peroxide ligand to yield the putative bis(μ-oxo)$Mn^{III}Mn^{IV}$ oxidant. However, in this case H_2O_2 was reacted (in silico) with class Ib RNRs, rather than O_2, and no experimental support for this postulate was available. [6]

The postulated peroxido-$Mn^{II}Mn^{III}$ intermediate in class Ib RNRs has not been trapped and no spectroscopic evidence exists to support its

* Corresponding author.
E-mail address: aidan.mcdonald@tcd.ie (A.R. McDonald).
[1] Current address: Institute for Sustainable and Circular Chemistry, Universiteit Utrecht, Universiteitsweg 99, 3584 CG Utrecht, the Netherlands.
[2] Current address: Helmholtz-Zentrum Dresden-Rossendorf e.V., Institute of Resource Ecology, Bautzner Landstraße 400, 01328 Dresden, Germany.

https://doi.org/10.1016/j.jinorgbio.2024.112583
Received 2 April 2024; Received in revised form 26 April 2024; Accepted 30 April 2024
Available online 5 May 2024

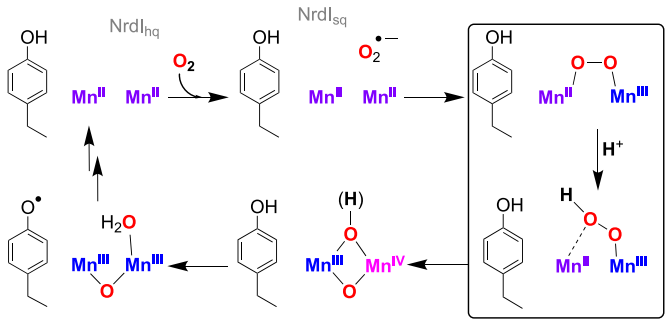

Scheme 1. Postulated catalytic cycle for class Ib RNRs.

formation (to the best of our knowledge). Furthermore, electron paramagnetic resonance (EPR) provides limited evidence for the formation of a bis(μ-oxo)$Mn^{III}Mn^{IV}$ species that was deemed responsible for tyrosine oxidation. [5] Fortunately, our group and others have developed synthetic Mn_2 complexes that replicate the structural and functional properties of class Ib RNRs. [7–9] We reported the Mn_2 complexes, $[Mn^{II}_2$(N-Et-HPTB)$(O_2CCH_3)](ClO_4)_2$ and $[Mn^{II}_2$(BPMP)$(O_2CCH_3)](ClO_4)$, (N-Et-HPTB = N,N,N′,N′-tetrakis(2-(1-ethylbenzimidazolyl))-2-hydroxy-1,3-diaminopropane; BPMP = 2,6-bis[(bis(2-pyridylmethyl)amino)methyl]-4-methylphenol) reacted with $O_2^{\bullet-}$ to form peroxido-$Mn^{II}Mn^{III}$ adducts (Fig. 1). Neither peroxido-$Mn^{II}Mn^{III}$ complex was capable of O—H bond activation and both were found to likely be precursors to a high-valent oxidant that would activate O—H bonds. Indeed, $[Mn_2(O_2)$(BPMP)$]^{2+}$ was activated either by reaction with an H^+-donor *or* thermally to yield a bis(μ-oxo)$Mn^{III}Mn^{IV}$ entity that was capable of phenol oxidation. [10] These complexes represented some of the first experimental support for the formation of a peroxido-$Mn^{II}Mn^{III}$ and a bis(μ-oxo)$Mn^{III}Mn^{IV}$ species in the catalytic cycle of Ib RNRs. Herein, we probe the formation of a peroxido-$Mn^{II}Mn^{III}$ complex supported by an alternative ligand and probe the H^+-activation of the peroxide-core further, demonstrating the formation of a $Mn^{II}Mn^{III}$ moiety that was capable of oxidative O—H activation.

2. Results and discussion

The polypyridine ligand TPDP (1,3-bis(bis(pyridin-2-ylmethyl)amino)propan-2-ol) was synthesized according to a reported procedure. [11] $[Mn^{II}_2$(TPDP)$(O_2CPh)_2](BPh_4)$ (**1**) was prepared by reaction of TPDP with $[Mn^{II}(O_2CCH_3)_2(H_2O)_4]$, benzoic acid, and triethylamine in methanol, followed by cation exchange with sodium tetraphenylborate ($NaBPh_4$, see supporting information for details, Scheme 2). [12] Crystals of **1** suitable for X-ray diffraction measurements were grown from cold CH_3CN (−30 °C) under inert conditions. The molecular structure of **1** showed two distorted 6-coordinate *pseudo*-octahedral Mn^{II} centers coordinated by TPDP and two benzoate ligands (Fig. 2). The structure was comparable to that obtained for $[Mn^{II}_2$(BPMP)$(O_2CCH_3)_2](ClO_4)$ and $[Mn^{II}_2$(BPMP)$(O_2CPh)_2](ClO_4)$ which both displayed two bridging carboxylate ligands coordinate to two Mn ions supported by an analogous polypyridine ligand. [13,14] The Mn/Mn separations in **1**, $[Mn^{II}_2$(BPMP)$(O_2CCH_3)_2](ClO_4)$, $[Mn^{II}_2$(BPMP)$(O_2CPh)_2](ClO_4)$ were

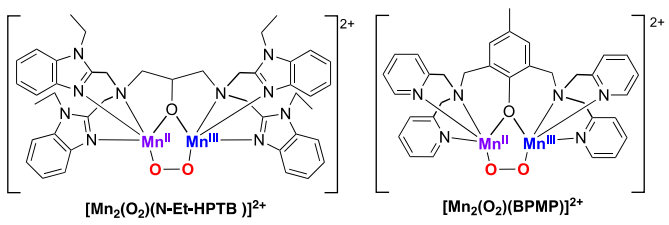

Fig. 1. Previously prepared peroxido-$Mn^{II}Mn^{III}$ complexes $[Mn_2(O_2)$(N-Et-HPTB)$]^{2+}$ (left) and $[Mn_2(O_2)$(BPMP)$]^{2+}$ (right).

3.3782(3), 3.41, and 3.48 Å, respectively (Table 1). [13,14] In contrast the Mn/Mn separation in the polybenzimidazole complex $[Mn^{II}_2$(N-Et-HPTB)$(O_2CCH_3)](ClO_4)_2$ was 3.6 Å. [8] The differences in Mn/Mn distances between the polypyridine and polybenzimidazole ligands are presumably as a result of the nature of the chelation of the pyridine donors versus the imidazole donors. Alternatively, $[Mn^{II}_2$(N-Et-HPTB)$(O_2CCH_3)](ClO_4)_2$ had just one bridging carboxylate ligand, while **1** and $[Mn^{II}_2$(BPMP)$(O_2CR)_2](ClO_4)$ contained two. **1** displayed a Mn/Mn distance shorter than that found in the native class Ib RNR enzymes, when a fully-reduced Mn^{II}_2 oxidation state was identified (3.7–3.9 Å, Table 1). When a Mn^{III}_2 oxidation state was observed, the Mn/Mn separation (3.3 Å) was closer to those of **1** and $[Mn^{II}_2$(BPMP)$(O_2CCH_3)_2](ClO_4)$. This can be rationalized as the higher oxidation state causing a contraction of the first coordination sphere. **1** is thus a reasonable structural mimic of the Mn_2 core of class Ib RNRs, albeit with a somewhat shorter inter-Mn distance.

High-resolution electrospray ionization mass-spectrometry (ESI-MS) analysis of **1** revealed a peak at m/z = 805.1790 that could be assigned to the $[Mn^{II}_2$(TPDP)$(O_2CC_6H_5)_2]^+$ cation (expected m/z = 805.1743, Fig. S1). Comparison of the Fourier transform infra-red (FT-IR) spectra of the free TPDP ligand and **1** revealed noticeable differences that indicated complexation had occurred (Figs. S2-S3). A broad feature at ν = 3300 cm^{-1} assigned to ν_{O-H} in TPDP was absent in the spectrum of **1**. Furthermore, signals that could be attributed to symmetric and asymmetric stretches of the carboxylate groups of the bridging benzoates were visible at $^{a/as}\nu_{C=O}$ = 1567/1381 cm^{-1}.

1 was dissolved in a mixture of CH_3CN/tetrahydrofuran (THF) (1:9, 1.5 mM) and cooled to −90 °C. Addition of a solution of KO_2 (0.04 M, 1 equiv.) solubilized with 2,2,2-cryptand (0.08 M, 4,7,13,16,21,24-hexaoxa-1,10-diazabicyclo[8.8.8]hexacosane) resulted in an immediate reaction according to electronic absorption spectroscopy (Fig. 3, S4). New absorption features were observed at λ_{max} = 450, 590 nm and the new species was defined as **2**. Addition of >1 equiv. of KO_2 resulted in less-than optimal yields of **2** and indicated the formation of other products as evidenced by new broader features according to electronic absorption spectroscopy (Fig. S5). **2** was a metastable species, with a half-life of $t_{1/2}$ = 2000 s at −90 °C.

The electronic absorption spectrum of **2** was similar to those of previously reported peroxido-$Mn^{II}Mn^{III}$ complexes (Fig. 4). [7,8,17] $[Mn_2(O_2)$(N-Et-HPTB)$]^{2+}$ displayed almost identical features at λ_{max} = 460, 610 nm, while $[Mn_2(O_2)$(BPMP)$]^{2+}$ presented an intense peak at λ_{max} = 440 nm and a weaker feature at λ = 590 nm. Therefore, due to the similarities with the two previously published species, we believe **2** should be assigned as a peroxido-$Mn^{II}Mn^{III}$ complex. In analogy to previously studied mononuclear peroxido-Mn^{III} complexes, it was postulated that the origin of the intense feature of λ_{max} ~ 440–460 nm was a peroxide-to-Mn^{III} charge transfer band and the less intense λ_{max} ~ 600 nm feature was derived from *d-d* transitions. [7,8,17] The high-energy features associated with peroxido-$Mn^{II}Mn^{III}$ species displayed molar absorption coefficients (ε) in the range of 300–500 M^{-1} cm^{-1}, while the lower-energy features displayed ε = ~200 M^{-1} cm^{-1}. Such ε-values have been previously observed as typical for mononuclear peroxido-Mn^{III} complexes. [7,8,17] This pair of spectroscopic features appears to be a fingerprint for peroxido-$Mn^{II}Mn^{III}$ complexes. The red-shift of the electronic features of polypyridine $[Mn_2(O_2)$(BPMP)$]^{2+}$ with respect to that of polypyridine **2** and polybenzimidazole $[Mn_2(O_2)$(N-Et-HPTB)$]^{2+}$ was indicative that the electronic environment of the peroxido-$Mn^{II}Mn^{III}$ core of $[Mn_2(O_2)$(BPMP)$]^{2+}$ was different. It is worth recalling that the XRD determined Mn/Mn separation in the Mn^{II}_2 starting materials did not agree with this trend, with the polybenzimidazole donor engendering a larger Mn/Mn separation. We postulate that this indicates that the bridging-alkoxide/phenoxide ligand, rather than the terminal pyridine/benzimidazole ligands, may have a greater influence over the electronic structure in such complexes.

ESI-MS analysis of a just-thawed solution of **2** showed a peak at m/z = 296.561 that was consistent with the dictation $[Mn_2(O_2)$(TPDP)$]^{2+}$

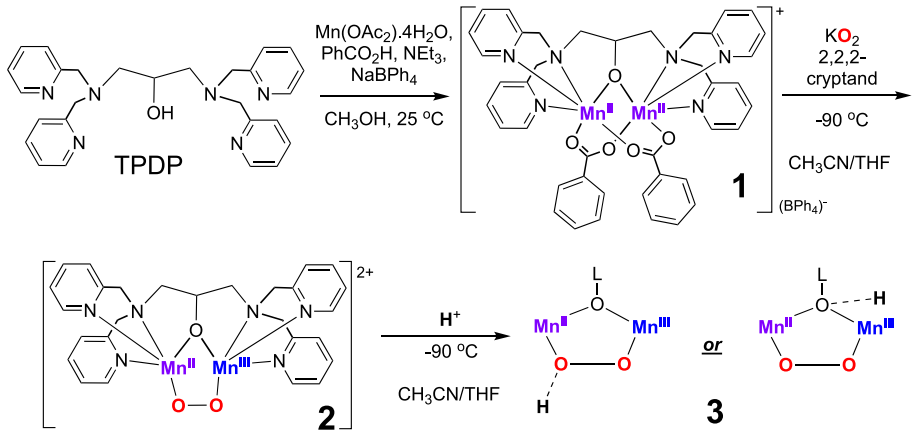

Scheme 2. Preparation of complexes **1**, **2**, and **3**.

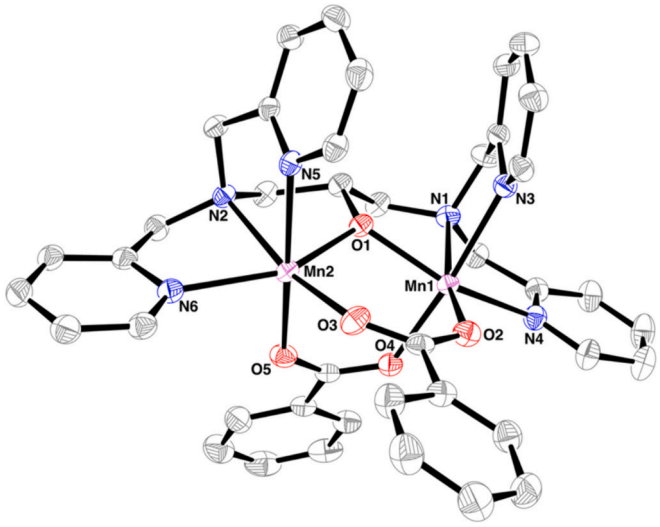

Fig. 2. ORTEP of **1**. Hydrogen atoms, BPh_4 counterion, and two CH_3CN molecules were omitted for clarity. Ellipsoids depicted at 50% probability.

(expected m/z = 296.5526, Fig. S6). In the observed mass ion, both of the benzoate ligands were absent. A similar observation was found for $[Mn_2(O_2)(N\text{-Et-HPTB})]^{2+}$ and $[Mn_2(O_2)(BPMP)]^{2+}$, where the bridging carboxylate ligands found in the precursor complex was absent in the ESI-MS spectrum of the peroxido-$Mn^{II}Mn^{III}$ entity. [7,8] Based on this, we surmise that the benzoate ligands are no longer bound in **2**. It is important to note that the m/z = 296.561 feature was not observed in the ESI-MS of **1**. This shows that this mass peak is associated with **2** and is not simply an adduct of the starting material and adventitious O_2.

Electron paramagnetic resonance (EPR) spectroscopy measurements of **2** at 2 K revealed a 22-line signal centered at $g \sim 2$ (Fig. 5, S7). This led us to assign **2** as a mixed-valent $Mn^{II}Mn^{III}$ complex. In a system with two ^{55}Mn equivalent centers and a S = ½ ground state, 11-lines would be expected in an isotropic environment based on the number of resonances being defined as $2nI + 1$ (n = #Mn ions, ^{55}Mn I = 5/2). In a system where the two Mn atoms are non-equivalent, such as a formally $Mn^{II}Mn^{III}$ complex, this could potentially yield a 36 line isotropic signal ($(2nI_1 + 1)(2mI_2 + 1) = 6*6 = 36$). [10,18,19] The number of lines would increase further should the signal be anisotropic. In practice, for $Mn^{II}Mn^{III}$ complexes ~20–30 features are observed due to overlap of the lines. EPR spectra of Mn_2 complexes with >20 lines and a wide spectral width are generally indicative of the formation of a mixed valent $Mn^{II}Mn^{III}$ species, rather than a mixed-valent $Mn^{III}Mn^{IV}$ complex, which typically displays fewer features (normally 16) over a narrower spectral width (100–150 mT). The yield of **2** was determined by EPR integration to be 65% ± 20% (using a Cu^{II} salt as a reference). We observed similar yields for $[Mn_2(O_2)(N\text{-Et-HPTB})]^{2+}$ and $[Mn_2(O_2)(BPMP)]^{2+}$.

Curiously, the EPR of **2** was remarkably similar to that of polybenzimidazole-supported $Mn^{II}Mn^{III}$ complex $[Mn_2(O_2)(N\text{-Et-HPTB})]^{2+}$, despite having different supporting ligands. [8] In contrast, the more closely related polypyridine supported $[Mn_2(O_2)(BPMP)]^{2+}$ displayed a broader spectral width than **2** and $[Mn_2(O_2)(N\text{-Et-HPTB})]^{2+}$. [7] This contrast in properties mirrored the electronic absorption spectroscopy observations, where **2** and $[Mn_2(O_2)(N\text{-Et-HPTB})]^{2+}$ were comparable, and $[Mn_2(O_2)(BPMP)]^{2+}$ was an outlier. These observations support the postulate that the electronic structure of the peroxido-$Mn^{II}Mn^{III}$ core appears to be influenced more by the nature of the bridging alkoxide/phenoxide ligands than the N-donors.

Mn K-edge X-ray absorption near edge spectroscopy (XANES) was performed on frozen samples of **1** and **2** in order to understand the Mn oxidation states and local electronic structure (Fig. 6). The low-valent complex **1** showed a rising edge with a first inflection at 6547.2 eV. For **2**, the first inflection point of the rising edge was determined to be 6549.3 eV, thus indicating an edge energy shift of 2.1 eV upon conversion of **1** to **2**. Typically, an increase of one in the formal oxidation of Mn is associated with an edge energy shift of 2–4 eV. [20–22] A shift of 2.1 eV, is therefore consistent with the average + 0.5 increase in Mn oxidation state on the conversion of a Mn_2^{II} species to a mixed-valent $Mn^{II}Mn^{III}$ species and agrees with the EPR data of **2**. Similar edge shifts were observed for $[Mn_2(O_2)(BPMP)]^{2+}$ and $[Mn_2(O_2)(N\text{-Et-HPTB})]^{2+}$ (Table 2). [7,8]

The pre-edge areas for features found at ~6540 eV in **1** and **2** were calculated to be 15.2 and 8.8 units, respectively (Figs. S8-S9). The pre-edge is associated with a symmetry-forbidden crystal field transition from the core 1 s orbitals to the 3d levels, which can gain some 4p character and thus intensity depending on the deviation from centrosymmetry. [23] This results in complexes with more distorted geometries displaying larger pre-edge areas than those with less distorted ones. The pre-edge peak areas imply that the Mn centers in **2** had a more centrosymmetric geometry in comparison to those of **1**. One possibility

Table 1
Comparison of Mn^{II}/Mn^{II} distances (Å) and Mn coordination numbers for class Ib RNRs and synthetic models (supporting ligands listed).

	Mn/Mn (Å)	Coordination #	Reference
1	3.378 (3)	6, 6	This work
Et-N-HTBP[a]	3.60	5, 5	[8]
BPMP[b]	3.41	6, 6	[13,14]
BPMP[c]	3.48	6, 6	[13,14]
B. subtilis	3.7	6, 5	[15]
E. coli	3.9	6, 6	[16]
C. ammoniagenes[d]	3.3	6, 5	[6]

[a] $[Mn^{II}_2$(N-Et-HPTB)$(O_2CCH_3)](ClO_4)_2$.
[b] $[Mn^{II}_2$(BPMP)$(O_2CCH_3)_2](ClO_4)$.
[c] $[Mn^{II}_2$(BPMP)$(O_2CCPh)_2](ClO_4)$
[d] Mn^{III}_2 core.

is that the two benzoate bridges in **1** lead to larger distortions around the Mn^{II} centers - upon conversion to **2** the bridging benzoates appear to be displaced by an O_2^{2-} ligand according to ESI-MS, presumably resulting in greater symmetry at Mn. It is also notable that both **1** and $[Mn^{II}_2$(N-Et-HPTB)$(O_2CCH_3)]^{2+}$ displayed relatively large pre-edge areas, while that of $[Mn^{II}_2$(BPMP)$(O_2CCH_3)_2]^{+}$ was relatively small (Table 2). Upon conversion to their corresponding $Mn^{II}Mn^{III}$ complexes, the pre-edge area dropped for both **2** and $[Mn^{II}_2(O_2)$(N-Et-HPTB)$]^{2+}$ but increased for $[Mn^{II}_2(O_2)$(BPMP)$]^{2+}$. As with the electronic absorption and EPR analyses, the bridging ligand (alkoxide versus phenoxide) thus appears to play a determining role in electronic structure at the Mn_2 core, inducing lower centrosymmetry for the alkoxide bridged complexes and greater centrosymmetry for those with a phenoxide bridge. Finally, the rising edge of **1** also exhibited a feature at ~6552 eV that was characteristic of the presence of Mn^{II}_2 (previously identified in Mn_2 RNRs). [24] Noticeably, this shoulder decreased in intensity in the spectrum of **2**, consistent with the loss of Mn^{II}_2. In summary, a combination of electronic absorption, EPR, and X-ray absorption spectroscopies and mass spectrometry allow us to assign the conversion of a Mn^{II}_2 complex (**1**) to a new peroxido-$Mn^{II}Mn^{III}$ (**2**) upon reaction with superoxide.

The previously studied peroxide complexes $[Mn_2(O_2)$(N-Et-HPTB)$]^{2+}$ and $[Mn_2(O_2)$(BPMP)$]^{2+}$ were determined to be poor oxidants, incapable of reacting with substrates with weak O—H bonds such as 2,2,6,6-tetramethylpiperidin-1-ol (TEMPO-H) or phenols. [7,8] As with those complexes, **2** displayed no reaction when exposed to TEMPO-H (Fig. S10). The lack of reactivity observed for all peroxido-$Mn^{II}Mn^{III}$

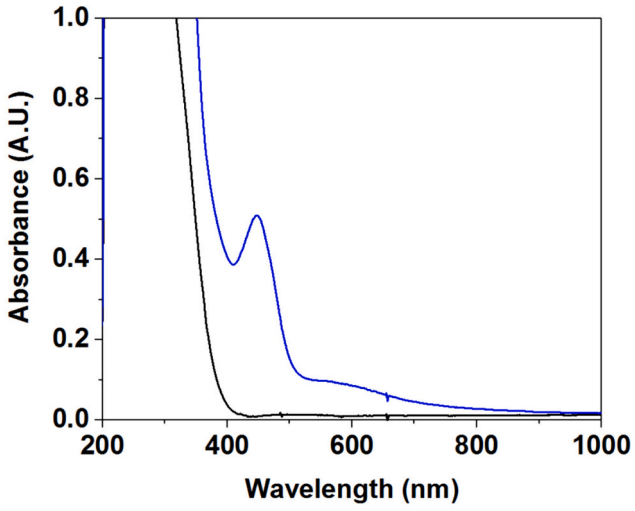

Fig. 3. Electronic absorption spectra of **1** (black trace, 1.5 mM) and **2** (blue trace, formed upon exposure of **1** to KO_2 (1 equiv.)) in 1:9 CH_3CN/THF at −90 °C. (For interpretation of the references to colour in this figure legend, the reader is referred to the web version of this article.)

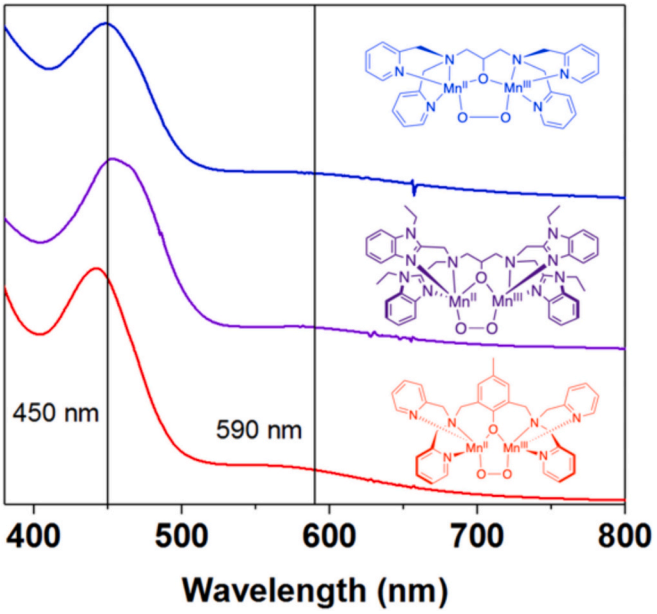

Fig. 4. Electronic absorption spectra of **2** (blue trace), $[Mn^{II}Mn^{III}(O_2)$(N-Et-HPTB)$]^{2+}$ (purple), and $[Mn^{II}Mn^{III}(O_2)$(BPMP)$]^{2+}$ (red). (For interpretation of the references to colour in this figure legend, the reader is referred to the web version of this article.)

(in our hands) appears to be intrinsic to this type of complex. As mentioned, it has been postulated that a proton donor is critical to class Ib RNR turnover, either to activate $O_2^{\bullet-}$ anion, facilitate O—O bond scission, or simply to enhance O—H bond activation reactivity. Critically, when both $[Mn_2(O_2)$(N-Et-HPTB)$]^{2+}$ and $[Mn_2(O_2)$(BPMP)$]^{2+}$ were exposed to H^+-donors, phenol and/or ferrocene were oxidized through presumed interception of a transient intermediate.

We previously identified *para*-toluenesulfonic acid (*p*-TsOH) as effective for the activation of peroxido-$Mn^{II}Mn^{III}$ cores. [10] To a solution of **2** (1.5 mM, 1:9 CH_3CN/THF) at −90 °C was added *p*-TsOH (2

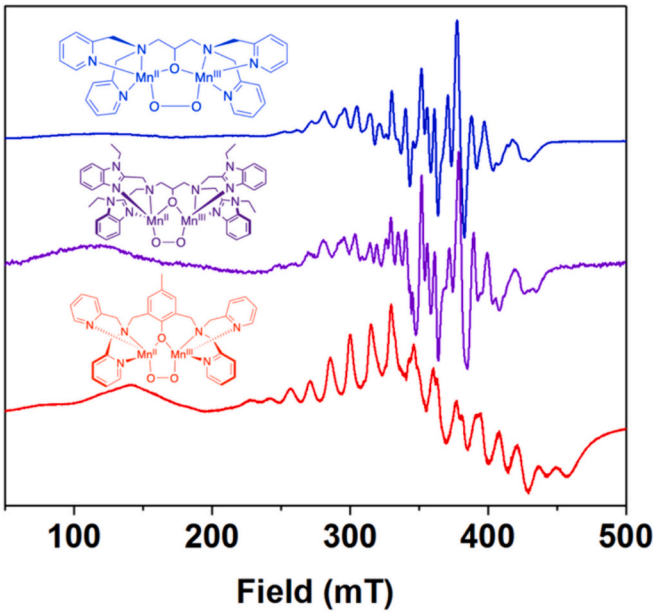

Fig. 5. X-Band EPR spectrum of **2** (blue trace), $[Mn_2(O_2)$(N-Et-HPTB)$]^{2+}$ (purple trace), and $[Mn_2(O_2)$(BPMP)$]^{2+}$ (red trace) all measured at 2 K, 9.65 GHz, 0.2 mW microwave power. (For interpretation of the references to colour in this figure legend, the reader is referred to the web version of this article.)

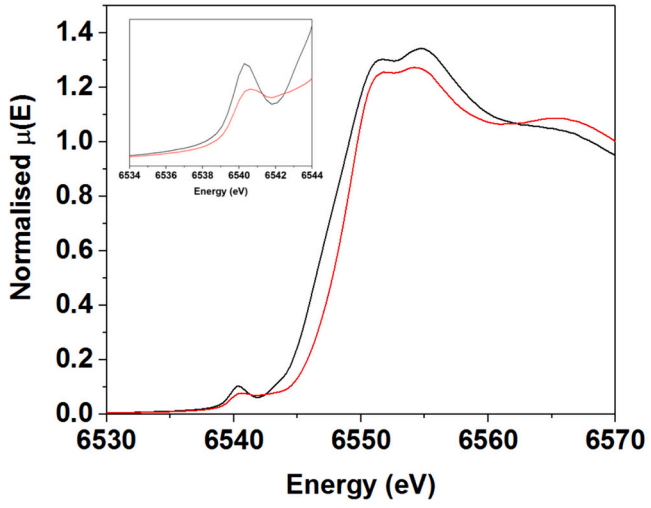

Fig. 6. Normalized XANES spectra of **1** (black trace) and **2** (red trace). Inset: Expansion of pre-edge region. (For interpretation of the references to colour in this figure legend, the reader is referred to the web version of this article.)

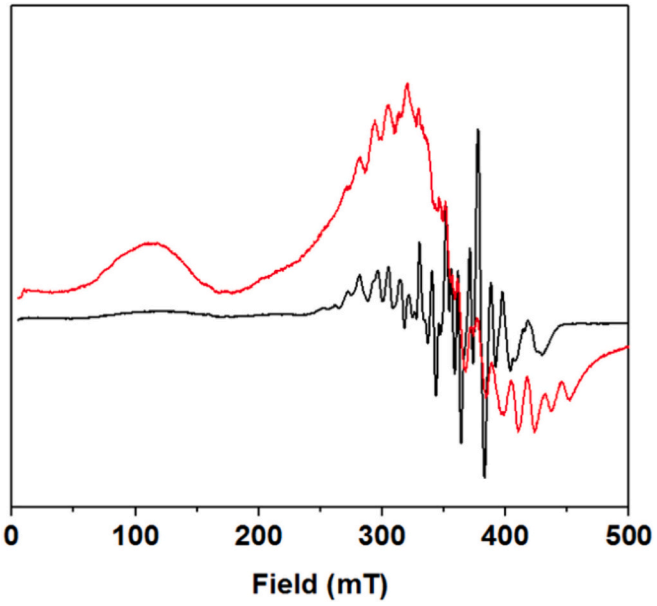

Fig. 7. X-Band EPR spectrum of **3** (red trace) and **2** (black trace) measured at 2 K (9.65 GHz, 0.2 mW microwave power). (For interpretation of the references to colour in this figure legend, the reader is referred to the web version of this article.)

equiv.). A slow reaction was observed that took 2000 s to complete, resulting in the formation of a new species (defined as **3**) according to electronic absorption features that tailed from the UV into the near-IR region (Fig. S11). The EPR spectrum of **3** revealed two new signals (Fig. 7), a broad feature centered at $g = 6.05$ and a 23-line signal centered at $g = 2$. The broad signal at a high g-tensor has been observed previously for $Mn^{II}Mn^{III}$ complexes and was assigned to transitions from the $S = 3/2$ state. [7,8,19,25] The 23-line signal at $g = 2$ was indicative of a $Mn^{II}Mn^{III}$ species (as described above), due to the high number of lines and broad spectral width. However, **3** displayed a relatively larger spectral width (200 mT) when compared to that measured for **2** (160 mT), indicating the formation of a novel $Mn^{II}Mn^{III}$ species. As with the previous $Mn^{II}Mn^{III}$ species trapped in our labs, the EPR spectra of **3** was not resolved and broadened significantly when measured at temperatures >10 K (Fig. S12). The yield of **3** was determined by EPR integration to be 50% ± 20% (using a Cu^{II} salt as a reference), with respect to the starting concentration of **1** in the reaction mixture. **3** displayed EPR features closer to those of $[Mn_2(O_2)(BPMP)]^{2+}$, rather than **2** and $[Mn_2(O_2)(N\text{-Et-HPTB})]^{2+}$ (Fig. 7, S13). As stated above, we postulate that the alkoxide/phenoxide bridge in these ligands appears to influence the electronic structure. We therefore conclude that the protonation event upon reaction between **2** and *p*-TsOH resulted in electronic structure changes comparable to replacing an alkoxide bridge in **2** and $[Mn_2(O_2)(N\text{-Et-HPTB})]^{2+}$ with a phenolate bridging ligand in $[Mn_2(O_2)(BPMP)]^{2+}$. We therefore tentatively suggest that the site of protonation is either the peroxide ligand or the alkoxide bridge linking the two manganese ions. This conclusion is based on our observations that the electronic structure of the Mn_2 core appears to be influenced predominantly by bridging ligands, rather than pyridine/benzimidazole donors of the supporting ligands.

To further analyze the Mn oxidation states and their local geometries, Mn K-edge XANES was performed on **3** (Fig. S14, Table 2). **3** displayed a rising edge with the first inflection at 6549.4 eV and a pre-edge peak centered at 6540.4 eV with an area of 3.9 units (Fig. S15). On first inspection, the XANES spectra of **2** and **3** appear very similar. The shift in edge energy was negligible (0.1 eV); as stated above, when an oxidation number increases by +1 at Mn, typically results in an edge energy shift between 2 and 4 eV. This indicated that **2** and **3** shared the same Mn oxidation states. Likewise, **2** and **3** displayed pre-edge peak energies of 6540.8 and 6540.4 eV, respectively. There was a modest decrease in the pre-edge area of **3** by 4.9 units relative to that of **2**, which supports increased centrosymmetry for the Mn centers of **3** compared to **2**. [23] Nam and co-workers described a hydroperoxido-Mn^{III} species generated from protonation of a peroxido-Mn^{III} that also exhibited a decrease in pre-edge area upon addition of the acid. [26] Therefore, we conclude that **3** contains the same $Mn^{II}Mn^{III}$ oxidation state as the $Mn^{II}Mn^{III}$-peroxide **2**, and tentatively ascribe the decrease in pre-edge area to protonation of the alkoxide ligand or peroxide bridge in **3** (Scheme 2).

Extended X-ray absorption fine structure (EXAFS) analysis on **2** and **3** was not carried out due to the poor solubility of **1** and the consequent low concentrations of **2** and **3**. The optimal conditions for the preparation of **2** and **3** were at [Mn] = 1.5 mM. At higher [Mn], relatively low yields of **2** were obtained. We observed the same for $[Mn_2(O_2)(BPMP)]^{2+}$ and $[Mn_2(O_2)(N\text{-Et-HPTB})]^{2+}$. [7,8] Such [Mn] concentration is less-than-ideal for EXAFS data collection. Furthermore, we observed photo-bleaching of these samples after periods of exposure to the beam, requiring us to perform relatively rapid data-collections on multiple spots. Again, this prevented collection of reliable EXAFS data. We were unable to measure the vibrational properties (through infra-red or Raman spectroscopies) of **2** and **3**. We were hindered in this effort because resonances of interest (ν_{O-O}, ν_{Mn-O}) were likely covered by solvents (CH_3CN *and* THF), and/or 2,2,2-cryptand, and/or ligand signals. We attempted Raman analysis of **2** and **3** using a variety of lasers with differing excitation wavelengths, however, we only identified

Table 2
Comparison of the XANES parameters of complexes **1**, **2**, **3**, **and related complexes**. [7,8].

Complex	Edge energy (eV)	Pre-edge area (units)	Pre-edge energy (eV)
1	6547.2	15.2	6540.3
$[Mn^{II}_2(N\text{-Et-HPTB})(O_2CCH_3)]^{2+}$	6547.7	19.5	6540.4
$[Mn^{II}_2(BPMP)(O_2CCH_3)_2]^{+}$	6548.4	5.9	6540.3
2	6549.3	8.8	6540.8
$[Mn_2(O_2)(N\text{-Et-HPTB})]^{2+}$	6548.7	14.1	6540.5
$[Mn_2(O_2)(BPMP)]^{2+}$	6548.9	9.4	6540.3
3	6549.4	3.9	6540.4

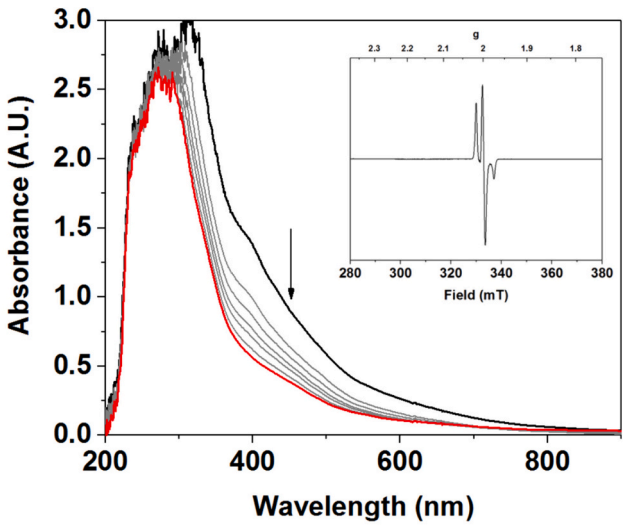

Fig. 8. Electronic absorption spectra of the reaction of **3** (black trace, 1.5 mM in 1:9 CH_3CN/THF) with TEMPO-H (30 equiv., red trace) at −90 °C. Inset: X-Band EPR of the post-reaction mixture showing the formation of TEMPO radical (9.34 GHz, 2.00 mW microwave power, 77 K). (For interpretation of the references to colour in this figure legend, the reader is referred to the web version of this article.)

features that could be attributed to the solvent. Furthermore, the thermal instability of **2** and **3** prevented IR measurement.

The peroxido-$Mn^{II}Mn^{III}$ species **2**, $[Mn_2(O_2)(N\text{-Et-HPTB})]^{2+}$, and $[Mn_2(O_2)(BPMP)]^{2+}$ were found to be unreactive towards external substrates. In contrast, **3** (1.5 mM, CH_3CN/THF) reacted readily with a substrate containing a weak O—H bond (TEMPO-H (30 equiv.)) at −90 °C as evidenced by a slow bleaching of the electronic absorption features associated with **3** (Fig. 8). EPR analysis on the post-reaction mixture revealed a rhombic signal with $g_x = 2.02$, $g_y = 2.00$, and $g_z = 1.97$, that was assigned to the TEMPO (2,2,6,6- tetramethyl-piperidin-1-yl)oxyl) radical. This signal has been observed previously following the oxidation of TEMPO-H by other oxidants. [10,27,28] The TEMPO radical yield was calculated to be 40 ± 15% by comparison to a TEMPO standard by EPR. Importantly, no signals that could be associated with Mn were identified in the post-reaction EPR. A control reaction resulted in a TEMPO radical yield of <5% (Fig. S16), implying that **3** was responsible for the oxidation.

We previously observed that the reaction between peroxido-$Mn^{II}Mn^{III}$ complex $[Mn_2(O_2)(BPMP)]^{2+}$ and a H^+-donor (*p*-TsOH) resulted in O—O bond scission and conversion to a bis(μ-O)$Mn^{III}Mn^{IV}$ species. [10] This bis(μ-O)$Mn^{III}Mn^{IV}$ complex was capable of the oxidation of a variety of substrates that contained a weak O—H bond (such as phenols). In contrast, addition of *p*-TsOH to peroxido-$Mn^{II}Mn^{III}$ complex **2** resulted in conversion to a new $Mn^{II}Mn^{III}$ species with no evidence for O—O bond scission. **3** was capable of O—H bond activation, albeit at considerably lower rates than the bis(μ-O)$Mn^{III}Mn^{IV}$ species, with a more activated substrate (TEMPO-H). Interestingly, **2** and other peroxido-$Mn^{II}Mn^{III}$ complexes showed no reactivity with the same substrates. This would suggest that class Ib RNRs likely rely on H^+-donors to facilitate tyrosyl radical generation, either via a (hydro)peroxido-$Mn^{II}Mn^{III}$ adduct or a bis(μ-O)$Mn^{III}Mn^{IV}$.[3] Due to the turgid rate of oxidation by **3**, we conclude that a bis(*μ*-oxo)$Mn^{III}Mn^{IV}$ species is likely employed in tyrosine activation by class Ib RNRs, although the current example demonstrates that a $Mn^{II}Mn^{III}$ entity is a plausible oxidant.

3. Conclusions

$[Mn^{II}_2(TPDP)(O_2CC_6H_5)_2](BPh_4)$ (**1**) was prepared and subsequently characterized via single-crystal X-ray diffraction, X-ray absorption, electronic absorption, and infrared spectroscopies, and mass spectrometry. **1** was a reasonable structural mimic of the Mn_2 core found in class Ib RNRs, displaying a comparable coordination environment and Mn/Mn separation. **1** was reacted with $O_2^{\bullet-}$ yielding a peroxido-$Mn^{II}Mn^{III}$ entity, **2**, that displayed electronic absorption, EPR, and XAS properties comparable to reported peroxido-$Mn^{II}Mn^{III}$ species. Reaction of **2** with an H^+-donor yielded another $Mn^{II}Mn^{III}$ species, **3**, rather than causing O—O bond scission according to electronic absorption, EPR, and XAS spectroscopies. **3** was deemed to contain a protonated alkoxide or hydroperoxide $Mn^{II}Mn^{III}$ core. Unlike all previous $Mn^{II}Mn^{III}$ species, **3** was capable of oxidative O—H activation, mirroring the generation of tyrosyl radical in class Ib RNRs. We conclude that class Ib RNRs rely on H^+-donors to facilitate tyrosyl radical generation, either via (hydro) peroxido-$Mn^{II}Mn^{III}$ or bis(μ-O)$Mn^{III}Mn^{IV}$ adducts - the current example demonstrates that a $Mn^{II}Mn^{III}$ entity is a credible oxidant.

CRediT authorship contribution statement

Lorna M. Doyle: Investigation. **Roel L.M. Bienenmann:** Investigation. **Robert Gericke:** Investigation. **Shuangning Xu:** Investigation. **Erik R. Farquhar:** Investigation. **Lawrence Que, Jr.:** Investigation. **Aidan R. McDonald:** Conceptualization.

Declaration of competing interest

The authors declare that they have no known competing financial interests or personal relationships that could have appeared to influence the work reported in this paper.

Data availability

Data will be made available on request.

Acknowledgements

This publication has emanated from research supported by the Irish Research Council (IRC) under grant numbers IRCLA/2022/2957 and GOIPG/2014/942. Research in the McDonald lab was supported in part by the European Union (ERC-2015-STG-678202) and research grants from Science Foundation Ireland (SFI/15/RS-URF/3307, SFI/17/RS-EA/3470). Support for this research in the Que lab has been provided by the US National Institutes of Health (5R35GM131721). XAS measurements at SSRL beamline 7-3 benefited from support of SSRL by the U.S. Department of Energy, Office of Science, Office of Basic Energy Sciences under Contract No. DE-AC02-76SF00515, as well as support of the SSRL Structural Molecular Biology Program through the DOE Office of Biological and Environmental Research and the National Institutes of Health (P30-GM-133894). Dr. Florian Molton and Prof. Carole Duboc (CNRS) are gratefully acknowledged for their support in collecting the EPR data reported in Fig. S12.

Appendix A. Supplementary data

Supplementary data to this article can be found online at https://doi.org/10.1016/j.jinorgbio.2024.112583.

References

[1] M. Eriksson, A. Jordan, H. Eklund, Biochemistry 37 (1998) 13359–13369.
[2] J. Stubbe, D.G. Nocera, C.S. Yee, M.C. Chang, Chem. Rev. 103 (2003) 2167–2201.
[3] M. Kolberg, K.R. Strand, P. Graff, K.K. Andersson, Biochim. Biophys. Acta 1699 (2004) 1–34.
[4] J.A. Cotruvo, J. Stubbe, Annu. Rev. Biochem. 80 (2011) 733–767.
[5] J.A. Cotruvo Jr., T.A. Stich, R.D. Britt, J. Stubbe, J. Am. Chem. Soc. 135 (2013) 4027–4039.
[6] N. Cox, H. Ogata, P. Stolle, E. Reijerse, G. Auling, W. Lubitz, J. Am. Chem. Soc. 132 (2010) 11197–11213.

[7] A.M. Magherusan, S. Kal, D.N. Nelis, L.M. Doyle, E.R. Farquhar, L. Que Jr., A. R. McDonald, Angew. Chem. Int. Ed. 58 (2019) 5718–5722.
[8] A.M. Magherusan, A. Zhou, E.R. Farquhar, M. García-Melchor, B. Twamley, L. Que, A.R. McDonald, Angew. Chem. Int. Ed. 57 (2018) 918–922.
[9] D.F. Leto, S. Chattopadhyay, V.W. Day, T.A. Jackson, Dalton Trans. 42 (2013) 13014–13025.
[10] L. Doyle, A. Magherusan, S. Xu, K. Murphy, E.R. Farquhar, F. Molton, C. Duboc, L. Que Jr., A.R. McDonald, Inorg. Chem. 63 (2024) 2194–2203.
[11] A. Trehoux, Y. Roux, R. Guillot, J.P. Mahy, F. Avenier, J. Mol. Catal. A 396 (2015) 40–46.
[12] Y.H. Dong, S. Menage, B.A. Brennan, T.E. Elgren, H.G. Jang, L.L. Pearce, L. Que, J. Am. Chem. Soc. 115 (1993) 1851–1859.
[13] S. Blanchard, G. Blondin, E. Riviere, M. Nierlich, J.J. Girerd, Inorg. Chem. 42 (2003) 4568–4578.
[14] M. Suzuki, M. Mikuriya, S. Murata, A. Uehara, H. Oshio, S. Kida, K. Saito, Bull. Chem. Soc. Jpn. 60 (1987) 4305–4312.
[15] A.K. Boal, J.A. Cotruvo Jr., J. Stubbe, A.C. Rosenzweig, Biochemistry 51 (2012) 3861–3871.
[16] A.K. Boal, J.A. Cotruvo Jr., J. Stubbe, A.C. Rosenzweig, Science 329 (2010) 1526–1530.
[17] D.F. Leto, T.A. Jackson, J. Biol. Inorg. Chem. 19 (2014) 1–15.
[18] C. Teutloff, K.O. Schafer, S. Sinnecker, V. Barynin, R. Bittl, K. Wieghardt, F. Lendzian, W. Lubitz, Magn. Reson. Chem. 43 (2005) S51–S64.
[19] H. Diril, H.-R. Chang, M.J. Nilges, X. Zhang, J.A. Potenza, H.J. Schugar, S.S. Isied, D.N. Hendrickson, J. Am. Chem. Soc. 111 (1989) 5102–5114.
[20] F. Farges, Phys. Rev. B 71 (2005) 155109.
[21] T.C. Weng, W.Y. Hsieh, E.S. Uffelman, S.W. Gordon-Wylie, T.J. Collins, V. L. Pecoraro, J.E. Penner-Hahn, J. Am. Chem. Soc. 126 (2004) 8070–8071.
[22] R.E. Schreiber, H. Cohen, G. Leitus, S.G. Wolf, A. Zhou, L. Que Jr., R. Neumann, J. Am. Chem. Soc. 137 (2015) 8738–8748.
[23] T.E. Westre, P. Kennepohl, J.G. DeWitt, B. Hedman, K.O. Hodgson, E.I. Solomon, J. Am. Chem. Soc. 119 (1997) 6297–6314.
[24] H.R. Rose, M.K. Ghosh, A.O. Maggiolo, C.J. Pollock, E.J. Blaesi, V. Hajj, Y. Wei, L. J. Rajakovich, W.C. Chang, Y. Han, M. Hajj, C. Krebs, A. Silakov, M.E. Pandelia, J. M. Bollinger Jr., A.K. Boal, Biochemistry 57 (2018) 2679–2693.
[25] L. Dubois, D.F. Xiang, X.S. Tan, J. Pecaut, P. Jones, S. Baudron, L. Le Pape, J. M. Latour, C. Baffert, S. Chardon-Noblat, M.N. Collomb, A. Deronzier, Inorg. Chem. 42 (2003) 750–760.
[26] H. So, Y.J. Park, K.B. Cho, Y.M. Lee, M.S. Seo, J. Cho, R. Sarangi, W. Nam, J. Am. Chem. Soc. 136 (2014) 12229–12232.
[27] G.B. Wijeratne, B. Corzine, V.W. Day, T.A. Jackson, Inorg. Chem. 53 (2014) 7622–7634.
[28] M. Lovisari, A.R. McDonald, Inorg. Chem. 59 (2020) 3659–3665.